Endocrinology. Author manuscript; available in PMC 2016 October 06.

Published in final edited form as:

Endocrinology. 2013 October ; 154(10): 3702–3718. doi:10.1210/en.2013-1155.

GSK-3β Function in Bone Regulates Skeletal Development, Whole-Body Metabolism, and Male Life Span

J. R. Gillespie, **J. R. Bush**, **G. I. Bell**, **L. A. Aubrey**, **H. Dupuis**, **M. Ferron**, **B. Kream**, **G. DiMattia**, **S. Patel**, **J. R. Woodgett**, **G. Karsenty**, **D. A. Hess**, and **F. Beier**

Department of Physiology and Pharmacology (J.R.G., J.R.B., G.I.B., L.A.A., H.D., D.A.H., F.L.B.), University of Western Ontario, London, Ontario, Canada; Children's Health Research Institute (J.R.G., J.R.B., L.A.A., H.D., F.B.), London, Ontario, Canada; Robarts Research Institute (G.I.B., D.A.H.), London, Ontario, Canada; Department of Genetics and Development (M.F., G.K.), Columbia University, New York, New York; Department of Medicine (B.K.), University of Connecticut Health Center, Farmington, Connecticut 06030; Cancer Research Laboratory Program (G.D.), Lawson Health Research Institute, Departments of Biochemistry and Oncology, University of Western Ontario, London, Ontario, Canada; Samuel Lunenfeld Research Institute/Mt Sinai Hospital (S.P., J.R.W,), Toronto, Ontario, Canada; Institut de recherches cliniques de Montréal (M.F.), Montréal, Canada H2W 1R7, and Institut de recherches cliniques de Montréal (M.R.), Montréal, Canada H2W 1R7

Abstract

Glycogen synthase kinase 3 β (GSK-3β) is an essential negative regulator or "brake" on many anabolic-signaling pathways including Wnt and insulin. Global deletion of GSK-3β results in peri-natal lethality and various skeletal defects. The goal of our research was to determine GSK-3β cell-autonomous effects and postnatal roles in the skeleton. We used the 3.6-kb *Col1a1* promoter to inactivate the *Gsk3b* gene (*Col1a1-Gsk3b* knockout) in skeletal cells. Mutant mice exhibit decreased body fat and postnatal bone growth, as well as delayed development of several skeletal elements. Surprisingly, the mutant mice display decreased circulating glucose and insulin levels despite normal expression of GSK-3β in metabolic tissues. We showed that these effects are due to an increase in global insulin sensitivity. Most of the male mutant mice died after weaning. Prior to death, blood glucose changed from low to high, suggesting a possible switch from insulin sensitivity to resistance. These male mice die with extremely large bladders that are preceded by damage to the urogenital tract, defects that are also seen type 2 diabetes. Our data suggest that skeletal-specific deletion of GSK-3β affects global metabolism and sensitizes male mice to developing type 2 diabetes.

The bones of the skeleton are formed through either endochondral or intramembranous ossification (reviewed in Refs. 1–3). Most of the skeleton forms through endochondral ossification in which a cartilage scaffold is produced by chondrocytes before being converted to bone by osteoblasts. Growth plate chondrocytes are found at either end of long

---

Address all correspondence and requests for reprints to: Frank Beier, Department of Physiology & Pharmacology, University of Western Ontario, London, Ontario, Canada; N6A 5C1. fbeier@uwo.ca.

Disclosure Summary: The authors confirm that there are no conflicts of interest.

bones surrounded by the perichondrium and are arranged in distinct layers of resting, proliferating, and hypertrophic cells, differing in gene expression patterns, rate of cell cycle progression, and cell morphology (reviewed in Refs. 3–6). Intramembranous ossification, in which preosteoblasts differentiate into mature osteoblasts to directly form bone without a cartilage template, occurs in cortical bone and the calvariae of the skull (reviewed in Ref. 7). Thus, the skeleton is a large and complex component of the body requiring precise autocrine, paracrine, and endocrine signaling to form properly.

Glycogen synthase kinase-3 (GSK-3) is an ubiquitous cellular regulator that functions as a "brake" in many anabolic pathways, including the Wnt/β-catenin and insulin pathways. GSK-3 has high protein kinase activity in resting tissues, is inhibited upon cellular stimulation, and negatively regulates many substrates. GSK-3α and GSK-3β are 51 kDa and 47 kDa, respectively, and are encoded by separate genes (reviewed in Refs. 8–10). Inhibition of GSK-3α or -β occurs through at least 2 mechanisms: direct phosphorylation (Ser21 and Ser9 of GSK-3α and β, respectively) by insulin/phosphatidylinositide 3-kinase/AKT signaling (11), or disruption/sequestration of the protein complex involved in canonical Wnt/β-catenin signaling (10). GSK-3α and -β appear functionally redundant in some pathways (12, 13), but unique and tissue-specific roles have also been demonstrated (14–18). Moreover, the relative roles of GSK-3 in mice may depend on genetic background or strain (19).

Skeletal phenotypes have been reported by others manipulating *Gsk3b* expression (20–22). Homozygous germ line deletion of *Gsk3b* causes a variable phenotype depending on genetic background, resulting in embryonic lethality (20) or survival to day of birth (P0) with cleft palate, bifid sternum, and delayed ossification of the sternum, skull, ear bones, and cranial base (21). In contrast, heterozygotes display increased ossification, clavicle abnormalities, and increased bone resorption (22). Delayed vs increased ossification appears to depend on *Gsk3b* dosage; however, these phenotypes are based on germ line loss of *Gsk3b*, and it is unclear whether these skeletal phenotypes are cell- or tissue-autonomous.

We previously reported the effects of pharmacologic inhibition of GSK-3 on tibia organ cultures ex vivo and chondrocyte-specific deletion of GSK-3β in vivo (23). Inhibition of both GSK-3α and -β increased bone growth ex vivo, consistent with GSK-3 negatively regulating anabolic pathways. However, cartilage-specific GSK-3β-deficient mice were phenotypically normal, except for displaying elevated GSK-3α protein levels. The lack of phenotype might be due to compensation by GSK-3α, suggesting that skeletal phenotypes in the global GSK-3β knockout (KO) mice (21) are likely due to functions of GSK-3β in other skeletal lineages, including osteoblasts. To address this possibility, we created mice in which GSK-3β was inactivated in early differentiating skeletal cells and osteoblasts.

Materials and Methods

Antibodies

The following antibodies were used: Cre ab24608, Sox9 ab3697 (Abcam); actin A5441, Runx2 R9403, insulin no. I2018 (Sigma Chemical Co.); goat antirabbit horseradish peroxidase (hrp) sc-2004, donkey antigoat hrp sc-2020, goat antimouse hrp sc-2005, Rankl

sc-9072, p57/Kip2 sc-8298 (Santa Cruz Biotechnology); GSK-3β no. 9315, pGSK-3β no. 9336, GSK-3α no. 9338, proliferating cell nuclear antigen (PCNA) no. 2586, cleaved caspase 3 no. 9661, β-catenin no. 9562 (Cell Signaling Technology). General chemicals and supplies were from Sigma and VWR.

Mouse breeding and genotyping

Mice homozygous for floxed *Gsk3b* alleles (*Gsk3b*$^{fl/fl}$) have been described elsewhere (18, 23, 24) and were crossed with mice expressing Cre recombinase under the control of an osteoblast-specific 3.6-kb fragment of the rat *Col1a1* promoter (*Cre*$^{+}$) (25, 26). Male *Gsk3b*$^{fl/+}$ *Cre*$^{+}$ mice were backcrossed with female *Gsk3b*$^{fl/fl}$ mice. The offspring from these crosses were analyzed. Mice on a 12-hour light-dark cycle were provided water and food ad libitum. All procedures involving animals were approved by the University of Western Ontario Animal Care and Use Committee. Cartilage-specific KO mice and PCR genotyping were described previously (23).

Skeletal staining

Skeletal staining was performed as described elsewhere (23, 27, 28). Briefly, skin and organs were removed, and the carcass was dehydrated in 95% ethanol overnight, followed by acetone overnight. Skeletons were stained with 0.015% Alcian Blue, 0.05% Alizarin Red, and 5% acetic acid in 70% ethanol for up to 4 days, and then cleared in 2% KOH overnight, 1% KOH for several days, and 0.5% KOH for approximately 1 week. Stained skeletons were stored in glycerol/ethanol (1:1). Images were captured with a Nikon SMZ1500 dissecting microscope and Photometrics Coolsnap camera using ImageMaster 5.0 software. At least 3 independent littermate pairs (control and knockout) were examined per time point. Representative images are shown.

Histology and immunohistochemistry (IHC)

Freshly dissected tibias from P0 and P21 mice were fixed in 4% paraformaldehyde overnight and embedded in plastic at The Centre for Bone and Periodontal Research (Montreal, Quebec-Canada) or decalcified with 0.1 M EDTA/PBS at 21°C before paraffin embedding and sectioning at the Robarts Research Institute Molecular Pathology Core Facility (London, Ontario, Canada). Plastic sections (5 μm) were stained with Von Kossa/toluidine blue. Paraffin sections (5 μm) were dewaxed in xylene followed by a graded alcohol series (100% ×2, 95%, 70%). Sections were stained with Picrosirius Red, Safranin O/Fast Green, or Von Kossa/toluidine blue. IHC sections were incubated in 3% H_2O_2 for 15 minutes at 21°C, then 10 mM sodium citrate at 95°C for 30 minutes, blocked with 5% goat serum in PBS (27–30), incubated with primary antibody overnight at 4°C, washed 4 times in PBS, and secondary antibody was applied according to manufacturers' recommendations. For detection, 3,3′-diaminobenzidine substrate was used with methyl blue counterstain. Images were captured with a Leica DME microscope and QImaging Micropublisher 5.0 RTV camera using QCapture Pro 5.1 software. Trabecular length was measured from the hypertrophic-bone interface to the end of the trabecular bone along the middle of the section. Terminal deoxynucleotide transferase-mediated dUTP nick end labeling (Calbiochem) and (Sigma) were performed essentially as per manufacturers' instructions. Representative images from at least 3 independent pairs of littermates are shown for each assay.

Western blot analyses

Calvaria, long bone cartilage, or organs were dissected from P0 or adult (2–6 months old) mice into cold Puck's solution A (23, 27, 31). Samples were flash frozen in radioimmune precipitation assay buffer, stored at −20°C overnight, and then homogenized, sonicated, centrifuged, and quantified. Protein (25–35 μg) was loaded per lane into precast NuPAGE Novex Midi Tris-Acetate Gels, and then separated and blotted using the XCell Surelock Mini-cell and Blot Module (Invitrogen) systems as per manufacturer's instructions. Blots were blocked in 5% BSA Tris-buffered saline-Tween 20 for 1 hour, probed with primary antibody overnight at 4°C, then incubated with appropriate hrp-conjugated secondary antibody 1 hour at 21°C, and signal detected with enhanced chemiluminescence (Amersham) using a ChemiImager 5500 system. Quantitative densitometry analysis was conducted by subtracting background and normalizing to β-actin signal. Results were converted relative to control, allowing comparison between blots by *t* test analysis. Representative blots from at least 3 independent experiments are shown. Bands separated by lanes that are not shown are displayed as separate but are from the same blot.

Blood glucose and metabolic measurements

Blood glucose was measured using a Contour glucose meter on tail vein blood. Nonfasted or random-fed readings were measured between 9 and 10 AM. Food was removed 6 hours before fasted readings. Mice were injected ip with 2.5g/kg body weight of glucose after fasting (glucose tolerance test [GTT]) or 0.2 U/kg body weight of insulin (insulin tolerance test [ITT]).

Serum readings were performed using a Millipore Multiplex system for the mouse bone panel 2A (catalog no. MBN2A-41K), Adiponectin-Single plex (Catalog no. MADPK-71K-ADPN), IGF-1 (catalog no. RMIGF187K), Glucagon (MENDO-75K), and GH (catalog no. EZRMGH) in the Screening Lab for Immune Disorders, St Joseph Hospital (London, Ontario, Canada). "Nondetectable" measurements were given the value 0.5 pm/mL below detection limit of assay. Serum carboxylation state of osteocalcin was measured as described previously (32).

Fat content analysis

Quantitative magnetic resonance (QMR) analyses were conducted using an Echo magnetic resonance imaging mobile unit at the Avian Facility for Advanced Research, Western University (London, Ontario, Canada). Displayed are absolute total body weight (scale), lean mass (QMR), and fat mass (QMR) from 2 male pairs and 3 female adult pairs (2–6 months old).

Statistical analysis

Data were collected from at least 3 independent pairs of littermates and expressed as mean ±SEM with $P < .05$ considered significant. *t* test analysis (GraphPad Prism 3.00 for Windows) was used to compare general measurements and Western blot densitometry data. Comparison of multiple measurements was performed using one-way ANOVA and a Tukey post test.

Results

Col1a1-driven *Gsk3b* inactivation

To study the role of *Gsk3b* in skeletal development, we crossed mice with conditional alleles of GSK-3β (*Gsk3b*$^{fl/fl}$) (18, 23, 24) with mice expressing Cre recombinase under control of the 3.6-kb fragment of the rat *Col1a1* promoter (25, 26). The following mouse genotype nomenclature is used throughout this paper: Control (Cont), *Gsk3b*$^{+/fl}$ *Cre*$^{-}$ and *Gsk3b*$^{fl/fl}$ *Cre*$^{-}$, Heterozygote (Het), *Gsk3b*$^{fl/+}$ *Cre*$^{+}$, and Knockout (KO), *Gsk3b*$^{fl/fl}$ *Cre*$^{+}$. Recombined DNA was detected by PCR (data not shown).

Western blot analyses revealed that Cre protein levels were high in KO calvarial tissue (bone) and, to a lesser extent, in growth plate cartilage of P0 KO mice (Figure 1A). Cre protein was undetectable by Western blot in control mice or other KO tissues, including heart (Figure 1A), brain, skin, and liver in P0 mice (data not shown). To further examine Cre expression, IHC was performed on P0 tibia sections. Cre protein was detected in the perichondrium and in cells of the trabeculas, with slight staining in prehypertrophic/hypertrophic cartilage (Figure 1A). Next, GSK-3β protein expression was examined to determine whether Cre expression corresponds to loss of GSK-3β protein. Quantitative densitometry of Western blots demonstrated that calvarial GSK-3β protein levels were reduced to 30%, which was confirmed by IHC (Figure 1B). GSK-3β protein was also reduced in cartilage (to 55% of control), specifically in late hypertrophic chondrocytes (Figure 1B).

To determine whether reduced GSK-3β protein would affect the activity of remaining GSK-3β, the levels of phosphorylation were examined. The amount of phosphorylated (inactive) GSK-3β was reduced in both KO calvariae (to 43% of control) and cartilage (to 62% of control) samples (Figure 1C), suggesting no major change in the proportion of active to inactive GSK-3β relative to controls. GSK-3α protein abundance was increased in KO cartilage, whereas GSK-3α was almost undetectable in bone lysates of either genotype (Figure 1D). These results suggest that GSK-3β ablation causes tissue-specific up-regulation of GSK-3α protein in growth plate cartilage, consistent with our earlier study (23), but not in bone.

Decreased weight, delayed postnatal bone growth, and altered growth plate morphology in *Col1a1-Gsk3b* KO mice

The number of KO mice born was slightly higher than the expected Mendelian ratio (47 KO mice of 154 total mice), demonstrating that KO mice are viable at birth. Of the 154 pups born, 17 died on P0, 13 of which were KO mice. Of the 4 control mice that died, 3 were victims of parental infanticide. KO mice that died within the first 12 hours appeared normal, fed, and did not appear to suffer from respiratory distress.

Surviving KO mice were significantly (11%) lighter than control littermates at P0 (Figure 2A). This difference in weight reached approximately 26% by P10, remaining relatively consistent (27%) at P21 (Figure 2A). Weight was not significantly different between heterozygote and control mice (Figure 2A).

We next examined the length of endochondral bones. Although not different at P0 or P10, KO tibias were approximately 15% shorter than controls at P21 (Figure 2B). Thus, reduced weight in KO mice precedes the reduction in bone length. We evaluated serum levels of IGF-1 and GH in adult (2–6 months) mice to determine whether reduced growth was associated with changes in these hormones; however, both were unchanged in the KO mice (data not shown).

The observed reduction of GSK-3β protein in growth plate cartilage (Figure 1B), along with decreased KO bone length (Figure 2B), prompted us to examine growth plate organization. Overall tibia and femur growth plate organization was similar in KO and controls at P0, although the hypertrophic zone was significantly increased in KO mice (Figure 2C, data not shown). Importantly, this phenotype was not present in our cartilage-specific *Gsk3b* mutants despite greater loss of GSK-3β, suggesting that these changes are not due to cartilage-autonomous processes.

Delayed skeletal development and ossification in *Col1a1-Gsk3b* KO mice

Skeletal malformations (eg, of palate and sternum) have been previously observed in global GSK-3β KO mice (21). Staining of P0 *Col1a1-Gsk-3b* KO skeletons with Alizarin Red (bone) and Alcian Blue (cartilage) demonstrated delayed hard palate closure and bifid sternum (Figure 3A), although these defects were less severe than those in germ line GSK-3β KO mice (21) and resolved by P21 (Figure 3A). These data suggest developmental delay rather than a developmental defect. However, mineralization of the Xiphoid process was absent in KO mice at P21 (Figure 3A, circled). Delayed hard palate closure did not affect the soft palate, and mice appeared to feed normally.

Several skeletal phenotypes not previously described in germ line GSK-3β KO mice were evident in *Col1a1-Gsk3b* KO mice. Limbs appeared morphologically normal in P0, P21, and 1-year old KO mice except for the underdeveloped and rounded deltoid tuberosity (Figure 3B, data not shown), which forms through endochondral bone formation and requires interactions between tendon and cartilage (33). Postnatal ossified structures of the knee joint, such as the patella and sesamoid bones, were much smaller in mutant mice (Figure 3C, circled). Delayed KO pelvic bone (endochondral) closure was also observed at P21 (Figure 3D, circled). KO P21 vertebrae were underdeveloped, with reduced spinous processes, and failed to fuse (Figure 3E). Other closure failures were apparent in the KO vertebrae, associated with false and floating ribs, as shown for T10 and T13 (Figure 3E). The most obvious defect was the absence of the large spinous process of the T2 vertebrae (Figure 3E, left). Thus, KO mice displayed numerous examples of developmentally delayed endochondral ossification.

Increased trabecular bone in *Col1a1-Gsk3b* KO mice

We next examined how *Gsk3b* deletion affects bone formation. Collagen production and bone formation/calcification were examined by Picrosirius Red and Von Kossa/toluidine blue staining of tibias at P0 (Figure 4A) and P21 (Figure 4B). Picrosirius Red and von Kossa staining showed that trabecula length was nearly doubled in KO mice at P0 (Figure 4A, data not shown). The middiaphysis of KO tibias also displayed increased mineralized trabecular

bone (Figure 4A, circled and transverse section). Trabecula length remains significantly increased at P21, although less dramatic (25%; Figure 4B), but the middiaphysis trabecular mineralization was normal (data not shown).

To elucidate the mechanisms underlying these phenotypes, we examined β-catenin, a GSK-3β-regulated mediator of canonical Wnt signaling known to control endochondral ossification (34–38). β-Catenin was increased in both cartilage and calvarias of mutant mice (Figure 4C), suggesting that skeleton-specific ablation of GSK-3β increases canonical Wnt/β-catenin signaling in both cartilage and bone.

Sox9 (39–41) and Runx2 (22, 42) are transcription factors essential for chondrocyte and osteoblast differentiation, respectively, and are regulated directly by GSK-3β or β-catenin. We observed tissue-specific up-regulation of Sox9 in cartilage, as well as bone-specific increase of Runx2 protein in our KO mice (Figure 4D). Thus, GSK-3β regulates the expression of key transcription factors for cartilage and bone development.

We next investigated cell cycle regulation in skeletal cells. Mutant osteoblasts displayed increased proliferation determined by increased PCNA and decreased staining for P57, a marker of cell cycle exit (Supplemental Figure 1, A and B, published on The Endocrine Society's Journals Online web site at http://endo.endojournals.org), which could account for increased trabecular bone in KO mice. Growth plate chondrocytes demonstrated increased PCNA staining through the proliferating zone and increased P57 staining in the prehypertrophic zone, indicating that more cells exited the cell cycle and become hypertrophic (Supplemental Figure 1, A and B). Furthermore, late hypertrophic chondrocytes displayed decreased apoptosis (cleaved caspase 3, terminal deoxy-nucleotide transferase-mediated dUTP nick end labeling) (Supplemental Figure 1C). These results could explain the larger hypertrophic zone despite smaller bones in the KO mice, because increased rates of proliferation and cell cycle exit would cause more cells to enter hypertrophy. However, the hypertrophic chondrocytes do not turn over to bone as rapidly, trapping them in hypertrophy and reducing bone elongation.

Decreased fat content in *Col1a1-Gsk3b* KO mice

Col1a1-Gsk3b KO mice are dwarfed with shorter bones than control mice, which is in contrast to our ex vivo studies in which bone growth increased upon pharmacologic inhibition of GSK-3 (23). Interestingly, delayed *Col1a1-Gsk3b* KO skeletal growth occurred postnatally, preceded by weight reduction, suggesting a possible metabolic defect. Indeed, the reduction in length of skeletal elements (~13%) is not proportional to the reduction in weight (~25%) (Figure 5A). Given that body weight and skeletal length are correlated in mice (43, 44) and that *Col1a1-Gsk3b* KO bone length is less affected than whole body weight, the reduction in weight is likely due to changes in other tissues. A KO animal with severe weight reduction is shown with its littermate (Figure 5A). The mutant mouse is 62% lighter than the control, whereas limb and skull size are much less affected (Figure 5A). To further investigate the relationship between skeletal size and weight, we analyzed adult mice by quantitative magnetic resonance (QMR), which revealed that *Col1a1-Gsk3b* KO mice weighed an average of 10 g less than control littermates (Figure 5B). Fat mass was significantly decreased in KO mice by approximately 8 g, whereas lean mass was not

significantly different (Figure 5B). In addition, adipocytes were smaller in KO mice (Figure 5C), confirming that the difference in weight is not due to loss of skeletal tissue but almost entirely due to reduced fat in KO mice. Consistent with reduced body fat and metabolic deregulation, *Col1a1-Gsk3b* KO mice have lower serum levels of 2 adipocyte-derived hormones (50), leptin at P10 and in the adult (Figure 5D) and adiponectin at P10 (Figure 5E). Given the reduced fat content, we investigated whether mutant mice consume different amounts of food. Although there was a trend toward less food consumption in mutant mice, this was not statistically significant. Furthermore, when food consumption was standardized to animal weight, the mutant mice ingested the same amount of food as control mice (Supplemental Figure 2A).

Reduced glucose and insulin as a consequence of increased insulin sensitivity in *Col1a1-Gsk3b* KO mice

In light of these metabolic changes and recent findings describing osteoblasts as endocrine regulators of glucose metabolism (32, 45–48), we examined blood glucose levels. Interestingly, blood glucose levels of KO mice were significantly reduced at birth compared with controls, unlike chondrocyte-specific *Gsk3b* KO mice (23) that showed no changes in blood glucose levels (Figure 6A). Pronounced hypoglycemia is apparent in KO pups prior to first feeding (data not shown) and might contribute to the 30% mortality at P0. Adult female (but not male) mice showed a significant decrease in blood glucose after fasting for 6 hours. In contrast, both female and male mice had reduced nonfasted blood glucose levels. Reduced blood glucose in the fed state suggests that insulin and/or insulin sensitivity may be affected. Indeed, serum insulin was significantly lower in P0 and adult skeleton-specific GSK-3β KO mice of both genders (Figure 6B).

Whereas both *Col1a1-Gsk3b* KO mice and bone-specific insulin receptor KO mice display decreased circulating insulin, bone-specific insulin receptor KO mice have elevated blood glucose levels (32, 48). We performed glucose tolerance tests (GTTs) to gain insight into this discrepancy. Female KO and control mice responded similarly to glucose administration (Figure 6C), suggesting that the pancreatic response to elevated blood glucose is intact in *Col1a1-Gsk3b* KO mice. This conclusion is supported by the fact that both islet number and circumference were normal in mutant mice (Supplemental Figure 2, B and C).

Perplexed by the presence of both low glucose and low insulin levels in our mice, we next examined insulin sensitivity. Insulin tolerance tests (ITT) revealed that female *Col1a1-Gsk3b* KO mice are significantly more insulin sensitive than their control littermates (Figure 6C). Mutant mice had a stronger overall reduction in blood glucose levels in response to insulin injection and took significantly longer to return to baseline levels. Interestingly, in preliminary studies in which mice were injected with a high insulin dose (0.75 U/kg), blood glucose levels of KO animals dropped so low that seizures occurred and glucose injections were required for recovery, highlighting the sensitivity of *Col1a1-Gsk-3β* KO mice to insulin. In contrast, female cartilage-specific GSK-3β KO mice showed an insulin response similar to that of their control littermates (data not shown). Whereas differences in glucagon might contribute to prolonged low glucose following insulin injection, we found no significant differences between genotypes in glucagon levels (Figure 6D).

We examined GSK-3β protein levels in metabolically active tissue to exclude possible confounding effects due to aberrant Cre expression (Supplemental Figure 2D). GSK-3β protein levels in pancreas, liver, fat, muscle, and kidney were not significantly different between control and KO mice (Supplemental Figure 2D). Furthermore, ELISA detection of GSK-3β in the muscle (data not shown) and pancreas (Supplemental Figure 2E) revealed no significant differences between control and mutant mice. Expression of both the 2.3-kb and 3.6-kb *Col1a1* promoter-driven *Cre* transgenes have been reported in brain (49). We therefore examined Cre and GSK-3β protein levels in the brains of *Col1a1*(3.6-kb promoter)-*Gsk-3β* KO and control mice and found no significant difference in GSK-3β abundance (Supplemental Figure 2F). We also could not detect Cre protein in the KO brains (Supplemental Figure 2F), suggesting that aberrant loss of GSK-3β in the brains of *Col1a1-Gsk-3β* KO mice cannot explain the phenotypes observed.

Finally, we examined osteocalcin, because its under-carboxylated form has been identified as an osteoblast-derived hormone regulated by the insulin pathway (32, 47, 48). However, we could not detect changes in circulating total or carboxylated osteocalcin in 2–6 month-old mice (data not shown).

Male-specific postweaning mortality due to possible development of type 2 diabetes, kidney damage, and hydronephrosis in *Col1a1-Gsk3b* KO mice

One of the most surprising and dramatic phenotypes observed was the death of nearly all male *Col1a1-Gsk3b* KO mice between weaning and 7 months of age. Only 1 female *Col1a1-Gsk3b* and no *Col2a1-Gsk3b* KO mice died within this interval (Figure 7A) (23). This male-specific mortality resembles recent studies of low-birth weight (LBW) animals in which male mice expire due to diabetic complications (50, 51). Indeed, several nonfasted hypoglycemic male mice became hyperglycemic prior to their premature death (Figure 7B), with a maximum reading of 16.9 mmol/L. Furthermore, glucose was detectable in the urine of most of the male KOs prior to death (data not shown). However, prior to this unpredictable transition, the metabolic profile of both genders was similar.

We next sought to determine the basis of premature death in male KO mice. Three to 6 hours prior to their death, we noticed hunched posture and a hard abdominal mass, which was found to be a full, distended bladder (Figure 7C). The bladder volume was typically 5 times that of control littermates (Figure 7C). Histologic analyses demonstrated that the bladder musculature and shape were completely disrupted (Supplemental Figure 3A). However, bladders of apparently healthy male KO mice and female KO mice were similar to those of controls (Supplemental Figure 2A). To ensure that aberrant loss of GSK-3β in the bladder was not responsible for this phenotype, IHC was performed on tissue sections (Supplemental Figure 3B). The cells of the epithelial layer uniformly stained for cytoplasmic GSK-3β in both control and KO mice, whereas the lamina propria was stained more sporadically (Supplemental Figure 3B).

Because a urinary tract obstruction could cause a distended bladder, we examined the male urogenital tract from the external penis to the pelvic ureter in KO males. Male KO mice dying prematurely displayed a swollen corpus cavernosum filled with red blood cells (Supplemental Figure 3C and Figure 7D). The corpus cavernosum is associated with erectile

dysfunction and has been studied in obesity and type 2 diabetes in various mouse models (52–54). Interestingly, mildly enlarged bladders were present in KO mice humanely destroyed before displaying a hunched posture. GSK-3β staining in the layer of cells surrounding the cavity of the corpus cavernosum was similar in control and KO mice (Supplemental Figure 4A).

We next investigated whether KO mice displayed kidney damage consistent with type 2 diabetes. The kidneys of male *Col1a1-Gsk3b* KO mice displayed hallmarks of hydronephrosis, including distended calyces, dilated collecting duct renal pyramids, damaged tubule lining cells, poorly defined glomerular spaces, and luminal space filled with proteinaceous material (Figure 8). Kidney damage was also present in otherwise normal KO mice, indicating that hydronephosis precedes corpus cavernosum and bladder damage. GSK-3β expression was similar in the glomerulus and renal tubules of mutant and control mice (Supplemental Figures 2D and 4B).

Discussion

Although skeletal phenotypes have been reported for both heterozygous and homozygous *Gsk3b* ubiquitous KO mice (21, 22), these studies could not distinguish between skeleton-intrinsic and -extrinsic roles of GSK-3β. Additionally, early lethality of homozygote mutants precludes analyses of postnatal skeletal development and function (20, 21). Here we describe mice with skeleton-specific inactivation of *Gsk3b* that display both skeletal and metabolic phenotypes. At the first glance, many of the phenotypes observed in our mice appear contradictory, but we believe that these contradictory effects are due to the interplay between local, skeleton-intrinsic effects of GSK-3β deficiency and systemic changes in metabolic factors.

Mutant mice have decreased body mass compared with control littermates at birth, before bone length is different. Between birth and P10, KO mice gain approximately 25% less weight than controls whereas skeletal growth is normal. This suggests that subsequent dwarfism in the mutant, including delayed development of various other skeletal elements, is secondary to a general weight reduction. The reduction in bone growth remains less pronounced than the reduction in body weight at later stages. We postulate that local, skeleton-specific effects of GSK-3β ablation, particularly increased proliferation of both chondrocytes and osteoblasts, are responsible for this partial rescue of bone growth. Others have shown that haploinsufficiency of GSK-3β can partially rescue dwarfism caused by cGMP-dependent protein kinase II deficiency (57). At the molecular level, these activities are at least partially controlled by increased abundance of the transcription factors β-catenin, Sox9, and Runx2, all crucial for skeletal growth and development.

Interestingly, none of the growth plate phenotypes described here were observed in cartilage-specific *Gsk3b* KO mice (23), despite the fact that recombination in chondrocytes occurred earlier in development and with higher efficiency than in *Col1a1-Gsk3b* KO mice. Thus, the observed effects on chondrocyte proliferation, apoptosis, and protein expression are unlikely due to chondrocyte-autonomous mechanisms, but rather to altered signals from other cells. Based on the strong expression of Cre in the perichondrium and bone of our mice, it is likely

that aberrant signaling from these tissues contribute to growth plate changes in the mutants (58).

Body fat reduction upon skeleton-specific inactivation of the *Gsk3b* gene was surprising, although not completely unexpected, given recent findings that bone-derived signals control body metabolism (32, 48). Body growth reduction is accompanied, and may be caused, by reduced blood glucose levels, and it appears possible that death in P0 mutant mice represents extreme cases of this phenotype. We examined GSK-3β expression in multiple tissues to ensure that these effects are not due to "leaky" expression of Cre recombinase (26, 49) and found no evidence for spurious inactivation of the *Gsk3b* gene. Whereas we cannot completely rule out confounding issues due to low levels of aberrant *Cre* expression, our phenotype is remarkably complementary to osteoblast-specific insulin receptor KO mice (32, 48). In particular, the utilized Cre driver line has been shown to confer recombination in the brain (49), which could affect the observed phenotypes, but we found no evidence for either *Cre* expression or *Gsk3b* recombination in the brains of our mice. One potential explanation for this discrepancy is that the earlier study used a ROSA reporter line very sensitive to Cre activity; transient spurious activity at some point in brain development could induce recombination in one allele of the reporter gene that is then detectable for the remainder of the animal's life. Our mice also showed no alterations in levels of hormones ultimately controlled by the nervous system (eg, GH, IGF-1), suggesting normal brain function. Finally, neither increased male lethality nor metabolic differences have been reported in mice with deletion of GSK-3β in the brain (59). Together, these data strongly suggest that loss of osteoblast GSK-3β is the major reason for the observed metabolic phenotypes in *Col1a1-Gsk3b* KO mice.

Two potential, although not mutually exclusive, mechanisms could explain the decreased blood glucose levels in mutant mice. First, loss of GSK-3β, an anabolic "brake," should hyperactivate the insulin pathway, falsely signaling to cells that glucose is abundant and should be taken up. Given the relatively large proportion of the body that is skeleton, increased glucose uptake specifically by osteoblasts could feasibly lower overall blood glucose, thus reducing glucose availability to other cells. This model is supported by the fact that *Col1a1-Gsk3b* KO mice respond more strongly to injected insulin and are phenotypically opposite to mice carrying osteoblast-specific inactivation of the insulin receptor with respect to weight, size, blood glucose levels, trabecular bone formation, and Runx2 expression (32, 48).

A second potential explanation for the blood glucose and body metabolism defects observed in skeleton-specific GSK-3β KO mice is a change in a bone-derived signal (or signals). Given the severe blood glucose disruption in KO mice, it seems likely that altered insulin signaling in additional tissues contributes to the enhanced response, suggesting disruption of bone-derived endocrine signaling. Undercarboxylated osteocalcin has been identified as one such signal (47), but neither undercarboxylated or total osteocalcin levels are changed in KO mutant mice, and no effects associated with altered osteocalcin signaling, such as disrupted pancreatic histology, were observed. Therefore it seems that another, still unknown, factor contributes to increased insulin sensitivity in *Col1a1-Gsk3b* KO mice. Interestingly, an activating mutation in *AKT2* causes both hypoglycemia and lack of plasma insulin in

humans (60), resembling the *Col1a1-Gsk3b* KO mouse metabolic phenotype. Because AKT directly inhibits GSK-3 activity, the pathways involved in this human disease and our mutant mice might be related.

Another interesting but confusing finding was that *Col1a1-Gsk3b* KO mice die prematurely, which is reminiscent of LBW-induced male-specific diabetes and premature death in mice (50, 51, 61, 62). Indeed, our male mice show signs of type 2 diabetes, including increasing blood glucose as they age, urinary glucose, large bladder, and hydronephrosis (63, 64). Only mutant mice near death had large bladders, whereas kidney and urogenital damage were present in male KO mice humanely destroyed prior to signs of illness. Hydronephrosis and nephropathy are observed in mouse (65) and rat (66) models of type 2 diabetes, as well as in humans with diabetes (67) in whom kidney failure is a major cause of death (55). Male mice are more susceptible to developing diabetes (50, 56), and renal disease progresses faster in male humans with diabetes (68). Taken together, this suggests that the mice are dying of diabetic complications, including kidney damage, and that bladder enlargement represents the disease end stage.

In conclusion, skeletal-specific deletion of *Gsk3b* offers a novel model with which to study the role of GSK-3β in postnatal skeletal development. Our studies demonstrate systemic and skeleton-intrinsic roles for GSK-3β. Deletion of GSK-3β in bone leads to metabolic disease and premature death in males with apparent type 2 diabetic complications. The fact that we see these phenotypes upon skeleton-specific ablation of GSK-3β highlights the central role of bone in regulating body metabolism. Future investigation into the molecular mechanisms through which GSK-3β functions in this context will provide important insights relevant to both skeletal health and metabolic disorders.

Supplementary Material

Refer to Web version on PubMed Central for supplementary material.

Acknowledgments

This work was supported by grants from the Canadian Institutes of Health Research (CIHR) to F.B. (MOP no. 43899). J.R.G. was a recipient of a (CIHR) Frederick Banting and Charles Best Canada Graduate Scholarship-Doctoral Award, a scholarship from the Canadian Arthritis Network (CAN) and the Ontario Graduate Scholarship (OGS). J.R.B. is the recipient of postdoctoral fellowships from CIHR and the Children's Health Foundation, London, Ontario, Canada. F.B. was the recipient of a Canada Research Chair Award.. Work in the laboratory of J.R.W. is funded by CIHR (MOP no. 74711).

Abbreviations

GSK-3	glycogen synthase kinase-3
GTT	glucose tolerance test
hrp	horse-radish peroxidase
ITT	insulin tolerance test
IHC	immunohistochemistry

KO	knockout
P0	day of birth
P21	postnatal day 21
PCNA	proliferating cell nuclear antigen
QMR	quantitative magnetic resonance

References

1. Mackie EJ, Ahmed YA, Tatarczuch L, Chen KS, Mirams M. Endochondral ossification: how cartilage is converted into bone in the developing skeleton. Int J Biochem Cell Biol. 2008; 40:46–62. [PubMed: 17659995]
2. Olsen BR, Reginato AM, Wang W. Bone development. Annu Rev Cell Dev Biol. 2000; 16:191–220. [PubMed: 11031235]
3. Kronenberg HM. Developmental regulation of the growth plate. Nature. 2003; 423:332–336. [PubMed: 12748651]
4. Provot S, Schipani E. Molecular mechanisms of endochondral bone development. Biochem Biophys Res Commun. 2005; 328:658–665. [PubMed: 15694399]
5. Beier F. Cell-cycle control and the cartilage growth plate. J Cell Physiol. 2005; 202:1–8. [PubMed: 15389526]
6. Kobayashi T, Kronenberg H. Minireview: transcriptional regulation in development of bone. Endocrinology. 2005; 146:1012–1017. [PubMed: 15604211]
7. Kronenberg HM. The role of the perichondrium in fetal bone development. Ann NY Acad Sci. 2007; 1116:59–64. [PubMed: 18083921]
8. Patel S, Doble B, Woodgett JR. Glycogen synthase kinase-3 in insulin and Wnt signalling: a double-edged sword? Biochem Soc Trans. 2004; 32:803–808. [PubMed: 15494020]
9. Woodgett JR. Judging a protein by more than its name: GSK-3. Sci STKE. 2001; 2001:RE12. [PubMed: 11579232]
10. Doble BW, Woodgett JR. GSK-3: tricks of the trade for a multitasking kinase. J Cell Sci. 2003; 116:1175–1186. [PubMed: 12615961]
11. Cross DA, Alessi DR, Cohen P, Andjelkovich M, Hemmings BA. Inhibition of glycogen synthase kinase-3 by insulin mediated by protein kinase B. Nature. 1995; 378:785–789. [PubMed: 8524413]
12. Doble BW, Patel S, Wood GA, Kockeritz LK, Woodgett JR. Functional redundancy of GSK-3α and GSK-3β in Wnt/β-catenin signaling shown by using an allelic series of embryonic stem cell lines. Dev Cell. 2007; 12:957–971. [PubMed: 17543867]
13. Liu S, Fang X, Hall H, et al. Homozygous deletion of glycogen synthase kinase 3β bypasses senescence allowing Ras transformation of primary murine fibroblasts. Proc Natl Acad Sci USA. 2008; 105:5248–5253. [PubMed: 18367674]
14. Liang MH, Chuang DM. Differential roles of glycogen synthase kinase-3 isoforms in the regulation of transcriptional activation. J Biol Chem. 2006; 281:30479–30484. [PubMed: 16912034]
15. Kerkela R, Kockeritz L, Macaulay K, et al. Deletion of GSK-3β in mice leads to hypertrophic cardiomyopathy secondary to cardiomyoblast hyperproliferation. J Clin Invest. 2008; 118:3609–3618. [PubMed: 18830417]
16. McManus EJ, Sakamoto K, Armit LJ, et al. Role that phosphorylation of GSK3 plays in insulin and Wnt signalling defined by knockin analysis. Embo J. 2005; 24:1571–1583. [PubMed: 15791206]
17. Ciaraldi TP, Oh DK, Christiansen L, et al. Tissue-specific expression and regulation of GSK-3 in human skeletal muscle and adipose tissue. Am J Physiol Endocrinol Metab. 2006; 291:E891–898. [PubMed: 16757548]

18. Patel S, Doble BW, Macaulay K, Sinclair EM, Drucker DJ, Woodgett JR. Tissue-specific role of glycogen synthase kinase-3β in glucose homeostasis and insulin action. Mol Cell Biol. 2008; 28:6314–6328. [PubMed: 18694957]
19. Patel S, Macaulay K, Woodgett JR. Tissue-specific analysis of glycogen synthase kinase-3α (GSK-3α) in glucose metabolism: effect of strain Variation. PLoS One. 2011; 6:e15845. [PubMed: 21253590]
20. Hoeflich KP, Luo J, Rubie EA, Tsao MS, Jin O, Woodgett JR. Requirement for glycogen synthase kinase-3β in cell survival and NF-κB activation. Nature. 2000; 406:86–90. [PubMed: 10894547]
21. Liu KJ, Arron JR, Stankunas K, Crabtree GR, Longaker MT. Chemical rescue of cleft palate and midline defects in conditional GSK-3β mice. Nature. 2007; 446:79–82. [PubMed: 17293880]
22. Kugimiya F, Kawaguchi H, Ohba S, et al. GSK-3β controls osteogenesis through regulating Runx2 activity. PLoS ONE. 2007; 2:e837. [PubMed: 17786208]
23. Gillespie JR, Ulici V, Dupuis H, et al. Deletion of glycogen synthase kinase-3β in cartilage results in up-regulation of glycogen synthase kinase-3α protein expression. Endocrinology. 2011; 152:1755–1766. [PubMed: 21325041]
24. Tanabe K, Liu Z, Patel S, et al. Genetic deficiency of glycogen synthase kinase-3beta corrects diabetes in mouse models of insulin resistance. PLoS Biol. 2008; 6:e37. [PubMed: 18288891]
25. Cochrane RL, Clark SH, Harris A, Kream BE. Rearrangement of a conditional allele regardless of inheritance of a Cre recombinase transgene. Genesis. 2007; 45:17–20. [PubMed: 17211878]
26. Liu F, Woitge HW, Braut A, Kronenberg MS, Lichtler AC, Mina M, Kream BE. Expression and activity of osteoblast-targeted Cre re-combinase transgenes in murine skeletal tissues. Int J Dev Biol. 2004; 48:645–653. [PubMed: 15470637]
27. Wang G, Woods A, Agoston H, Ulici V, Glogauer M, Beier F. Genetic ablation of Rac1 in cartilage results in chondrodysplasia. Dev Biol. 2007; 306:612–623. [PubMed: 17467682]
28. Ulici V, Hoenselaar KD, Agoston H, et al. The role of Akt1 in terminal stages of endochondral bone formation: Angiogenesis and ossification. Bone. 2009; 45:1133–1145. [PubMed: 19679212]
29. Solomon LA, Li JR, Berube NG, Beier F. Loss of ATRX in chondrocytes has minimal effects on skeletal development. PLoS One. 2009; 4:e7106. [PubMed: 19774083]
30. Yan Q, Feng Q, Beier F. Endothelial nitric oxide synthase deficiency in mice results in reduced chondrocyte proliferation and endochondral bone growth. Arthritis Rheum. 2010; 62:2013–2022. [PubMed: 20506524]
31. Stanton LA, Sabari S, Sampaio AV, Underhill TM, Beier F. p38 MAP kinase signalling is required for hypertrophic chondrocyte differentiation. Biochem J. 2004; 378:53–62. [PubMed: 14594450]
32. Ferron M, Wei J, Yoshizawa T, et al. Insulin signaling in osteoblasts integrates bone remodeling and energy metabolism. Cell. 2010; 142:296–308. [PubMed: 20655470]
33. Blitz E, Viukov S, Sharir A, et al. Bone ridge patterning during musculoskeletal assembly is mediated through SCX regulation of Bmp4 at the tendon-skeleton junction. Developmental cell. 2009; 17:861–873. [PubMed: 20059955]
34. Holmen SL, Zylstra CR, Mukherjee A, et al. Essential role of beta-catenin in postnatal bone acquisition. J Biol Chem. 2005; 280:21162–21168. [PubMed: 15802266]
35. Chen M, Zhu M, Awad H, et al. Inhibition of β-catenin signaling causes defects in postnatal cartilage development. J Cell Sci. 2008; 121:1455–1465. [PubMed: 18397998]
36. Chen Y, Whetstone HC, Youn A, et al. Beta-catenin signaling pathway is crucial for bone morphogenetic protein 2 to induce new bone formation. J Biol Chem. 2007; 282:526–533. [PubMed: 17085452]
37. Baron R, Rawadi G. Targeting the Wnt/β-catenin pathway to regulate bone formation in the adult skeleton. Endocrinology. 2007; 148:2635–2643. [PubMed: 17395698]
38. Tamamura Y, Otani T, Kanatani N, et al. Developmental regulation of Wnt/beta-catenin signals is required for growth plate assembly, cartilage integrity, and endochondral ossification. J Biol Chem. 2005; 280:19185–19195. [PubMed: 15760903]
39. Akiyama H, Lyons JP, Mori-Akiyama Y, et al. Interactions between Sox9 and β-catenin control chondrocyte differentiation. Genes Dev. 2004; 18:1072–1087. [PubMed: 15132997]

40. Akiyama H, Chaboissier MC, Martin JF, Schedl A, de Crombrugghe B. The transcription factor Sox9 has essential roles in successive steps of the chondrocyte differentiation pathway and is required for expression of Sox5 and Sox6. Genes Dev. 2002; 16:2813–2828. [PubMed: 12414734]
41. Song JH, Kim JH, Park S, et al. Signaling responses of osteoblast cells to hydroxyapatite: the activation of ERK and SOX9. J Bone Miner Metab. 2008; 26:138–142. [PubMed: 18301969]
42. Komori T. Regulation of bone development and maintenance by Runx2. Front Biosci. 2008; 13:898–903. [PubMed: 17981598]
43. Hooper ACB. Effects of divergent selection for body-weight on bone length and diameter in mice. Anim Prod. 1977; 24:77–82.
44. Hooper ACB. Further Study of Effects of Selection for Relative Bone Length. J Anat. 1977; 124:495–496.
45. Fukumoto S, Martin TJ. Bone as an endocrine organ. Trends Endocrinol Metab. 2009; 20:230–236. [PubMed: 19546009]
46. Yoshizawa T, Hinoi E, Jung DY, et al. The transcription factor ATF4 regulates glucose metabolism in mice through its expression in osteoblasts. J Clin Invest. 2009; 119:2807–2817. [PubMed: 19726872]
47. Lee NK, Sowa H, Hinoi E, et al. Endocrine regulation of energy metabolism by the skeleton. Cell. 2007; 130:456–469. [PubMed: 17693256]
48. Fulzele K, Riddle RC, DiGirolamo DJ, et al. Insulin receptor signaling in osteoblasts regulates postnatal bone acquisition and body composition. Cell. 2010; 142:309–319. [PubMed: 20655471]
49. Scheller EL, Leinninger GM, Hankenson KD, Myers MG Jr, Krebsbach PH. Ectopic expression of Col2.3 and Col3.6 promoters in the brain and association with leptin signaling. Cells Tissues Organs. 2011; 194:268–273. [PubMed: 21555864]
50. Inoue T, Kido Y, Asahara S, et al. Effect of intrauterine undernutrition during late gestation on pancreatic β cell mass. Biomed Res. 2009; 30:325–330. [PubMed: 20051640]
51. Cox AR, Gottheil SK, Arany EJ, Hill DJ. The effects of low protein during gestation on mouse pancreatic development and β cell regeneration. Pediatr Res. 2010; 68:16–22. [PubMed: 20386490]
52. Carneiro FS, Giachini FR, Lima VV, et al. Adenosine actions are preserved in corpus cavernosum from obese and type II diabetic db/db mouse. J Sex Med. 2008; 5:1156–1166. [PubMed: 18221284]
53. Jin HR, Kim WJ, Song JS, et al. Functional and morphologic characterizations of the diabetic mouse corpus cavernosum: comparison of a multiple low-dose and a single high-dose streptozotocin protocols. J Sex Med. 2009; 6:3289–3304. [PubMed: 19732306]
54. Toque HA, da Silva FH, Calixto MC, et al. High-fat diet associated with obesity induces impairment of mouse corpus cavernosum responses. BJU Int. 2011; 107:1628–1634. [PubMed: 20942830]
55. Bakris GL. Recognition, pathogenesis, and treatment of different stages of nephropathy in patients with type 2 diabetes mellitus. Mayo Clin Proc. 2011; 86:444–456. [PubMed: 21531886]
56. Chow F, Ozols E, Nikolic-Paterson DJ, Atkins RC, Tesch GH. Macrophages in mouse type 2 diabetic nephropathy: correlation with diabetic state and progressive renal injury. Kidney Int. 2004; 65:116–128. [PubMed: 14675042]
57. Kawasaki Y, Kugimiya F, Chikuda H, et al. Phosphorylation of GSK-3β by cGMP-dependent protein kinase II promotes hypertrophic differentiation of murine chondrocytes. J Clin Invest. 2008; 118:2506–2515. [PubMed: 18551195]
58. Hinoi E, Bialek P, Chen YT, et al. Runx2 inhibits chondrocyte proliferation and hypertrophy through its expression in the perichondrium. Genes Dev. 2006; 20:2937–2942. [PubMed: 17050674]
59. Kim WY, Wang X, Wu Y, Doble BW, Patel S, Woodgett JR, Snider WD. GSK-3 is a master regulator of neural progenitor homeostasis. Nat Neurosci. 2009; 12:1390–1397. [PubMed: 19801986]
60. Hussain K, Challis B, Rocha N, et al. An activating mutation of AKT2 and human hypoglycemia. Science. 2011; 334:474. [PubMed: 21979934]

61. Chamson-Reig A, Thyssen SM, Arany E, Hill DJ. Altered pancreatic morphology in the offspring of pregnant rats given reduced dietary protein is time and gender specific. J Endocrinol. 2006; 191:83–92. [PubMed: 17065391]

62. Chamson-Reig A, Thyssen SM, Hill DJ, Arany E. Exposure of the pregnant rat to low protein diet causes impaired glucose homeostasis in the young adult offspring by different mechanisms in males and females. Exp Biol Med (Maywood). 2009; 234:1425–1436. [PubMed: 19657071]

63. Vadhavkar M, Golbidi S, Sea J, Longpre M, Stothers L, Laher I. Exercise improves bladder function in diabetic mice. Neurourol Urodyn. 2011; 30:174–182. [PubMed: 20860017]

64. Castro JC, Camargos AF, Goulart EA, Junqueira HS. Sonographic evaluation of bladder volume in diabetic children and adolescents compared with nondiabetic subjects. J Ultrasound Med. 2004; 23:1307–1313. [PubMed: 15448320]

65. Tesch GH, Lim AK. Recent insights into diabetic renal injury from the db/db mouse model of type 2 diabetic nephropathy. Am J Physiol Renal Physiol. 2011; 300:F301–310. [PubMed: 21147843]

66. Baynes J, Murray DB. Cardiac and renal function are progressively impaired with aging in Zucker diabetic fatty type II diabetic rats. Oxid Med Cell Longev. 2009; 2:328–334. [PubMed: 20716921]

67. Toyota N, Ogawa D, Ishii K, et al. Emphysematous cystitis in a patient with type 2 diabetes mellitus. Acta Med Okayama. 2011; 65:129–133. [PubMed: 21519371]

68. Jafar TH, Schmid CH, Stark PC, et al. The rate of progression of renal disease may not be slower in women compared with men: a patient-level meta-analysis. Nephrol Dial Transplant. 2003; 18:2047–2053. [PubMed: 13679479]

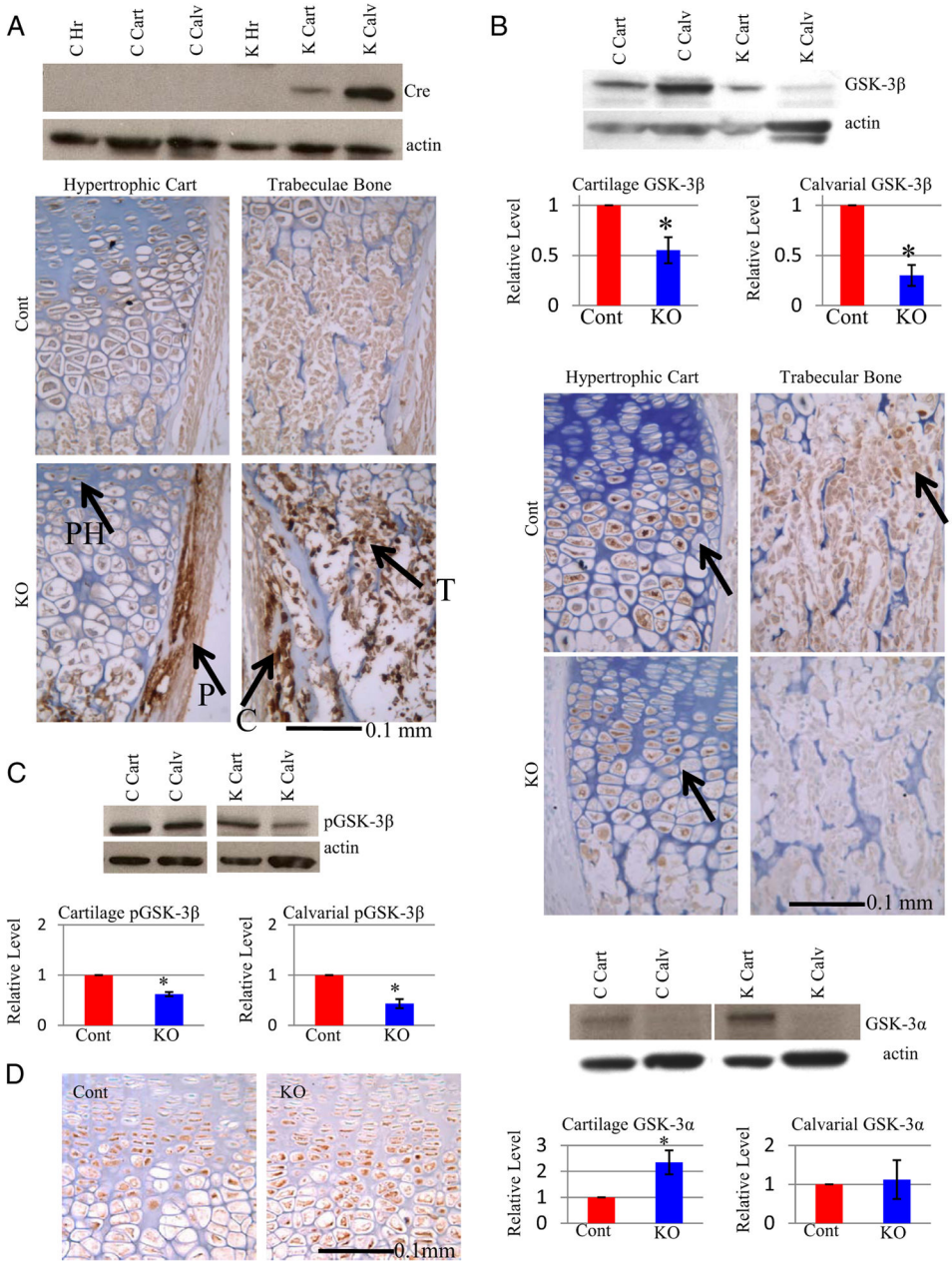

Figure 1.

Bone-Specific Inactivation of *Gsk3b* A, Analyses of Cre protein expression in skeletal tissue. Top: Western blot analyses of newborn (P0) protein extracts with Cre antibody (loading control β-actin) for control (*Gsk3b*$^{fl/fl}$ *Cre*$^{-}$ or *Gsk3b*$^{fl/+}$ *Cre*$^{-}$, C) and KO (*Gsk3b*$^{fl/fl}$ *Cre*$^{+}$; K) mice, using heart (Hr), cartilage (Cart), and calvarial (Calv) lysates. Bottom: IHC of P0 tibias shows that Cre protein is present in perichondrium (P), in trabeculae (T), prehypertrophic chondrocytes (PH), and cortical bone (C). B, GSK-3β protein expression in cartilage and bone tissue. B (top), Western blot analyses of P0 samples with antibodies to GSK-3β and quantitative densitometry results of cartilage (n = 8) (left) and calvariae (n = 8) (right) samples below. Bottom: GSK-3β IHC of P0 tibia sections. C,

Analyses of phosphorylation levels of GSK-3β protein. Top: Western blot analysis and Bottom: Densitometric quantification of pGSK-3β in control (C or Cont) or bone specific KO (K or KO) mice in cartilage (n = 4) (left) and calvariae (n = 4) (right). D, Analyses of GSK-3α protein levels in skeleton of bone-specific GSK-3β KO mice. Left: GSK-3α IHC of P0 tibia, with the prehypertrophic/hypertrophic growth plate zone displayed. Right: Densitometry of GSK-3α protein expression from Western blot analyses of cartilage (n = 8) and calvariae (n = 8) from control (Cont) and knockout (KO) mice (loading control β-actin). Quantitative data were compared using *t* test analysis; significant differences are denoted by asterisk (*, $P < .05$).

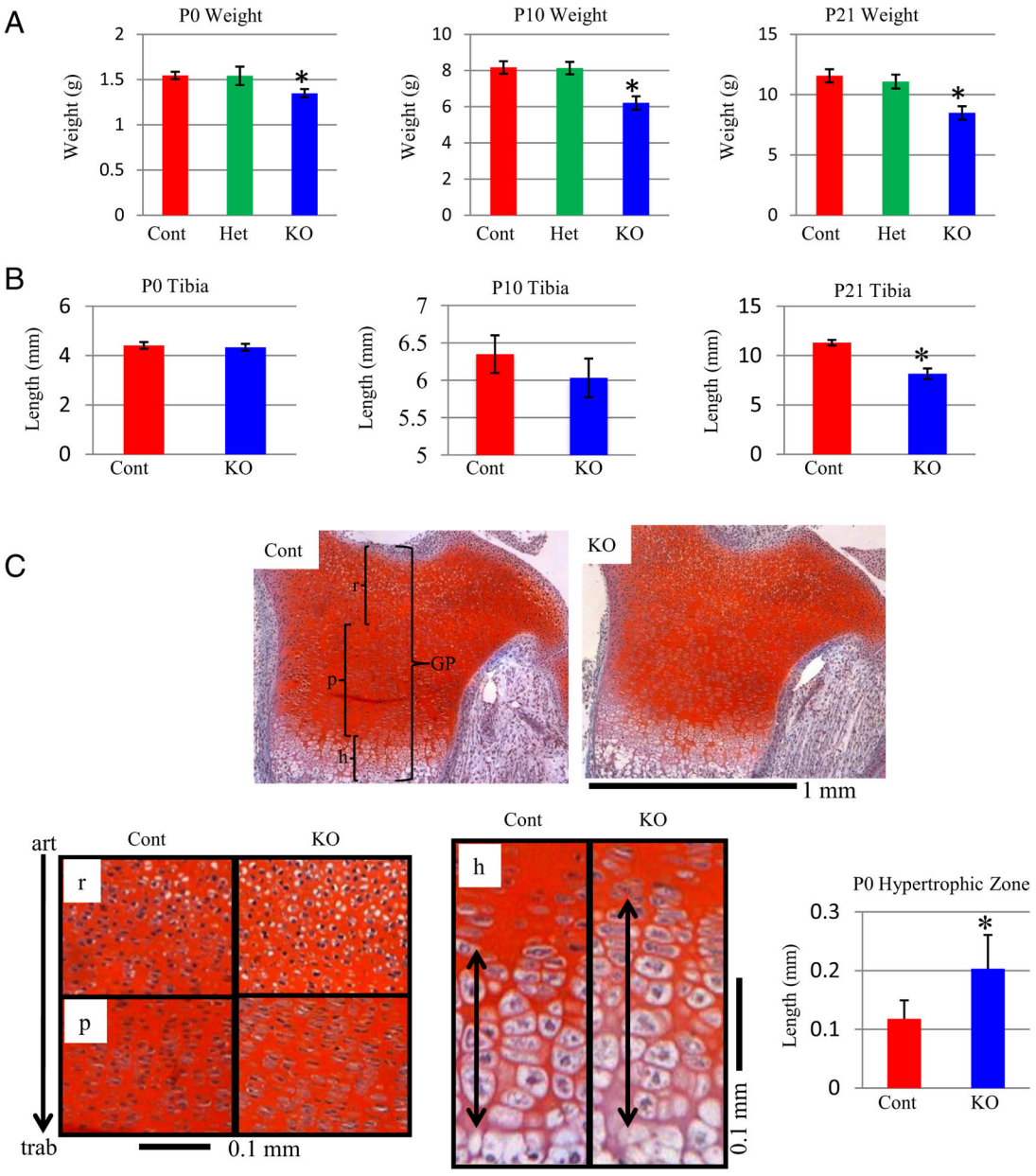

Figure 2.

Reduced Weight and Growth Plate Effects in *Col1a1-Gsk3b* KO Mice A, Comparison of postnatal mouse body weight. Weights of control (Cont), heterozygous (Het), and knockout mice (KO) were compared at P0 (n = 8) (left), P10 (n = 13) (middle), and P21 (n = 11) (right) by a one-way ANOVA with a Tukey posttest. B, Lengths of tibias were compared at P0 (n = 13) (left), P10 (n = 5) (middle), and P21 (n = 4) (bottom). C (top), Safranin O staining of cartilage (glycosaminoglycans stain red; GP, growth plate; r, resting zone; p, proliferating zone; h, hypertrophic zone). C (bottom), Higher magnification of growth plate zones, with the same orientation as in A (articular surface [art; top] and trabecular bone [trab]; bottom). C (bottom right), Length of hypertrophic (h) zone at P0. Statistical analysis

was conducted using *t* test (n = 6). Significant differences are denoted by asterisk (*, $P < .05$).

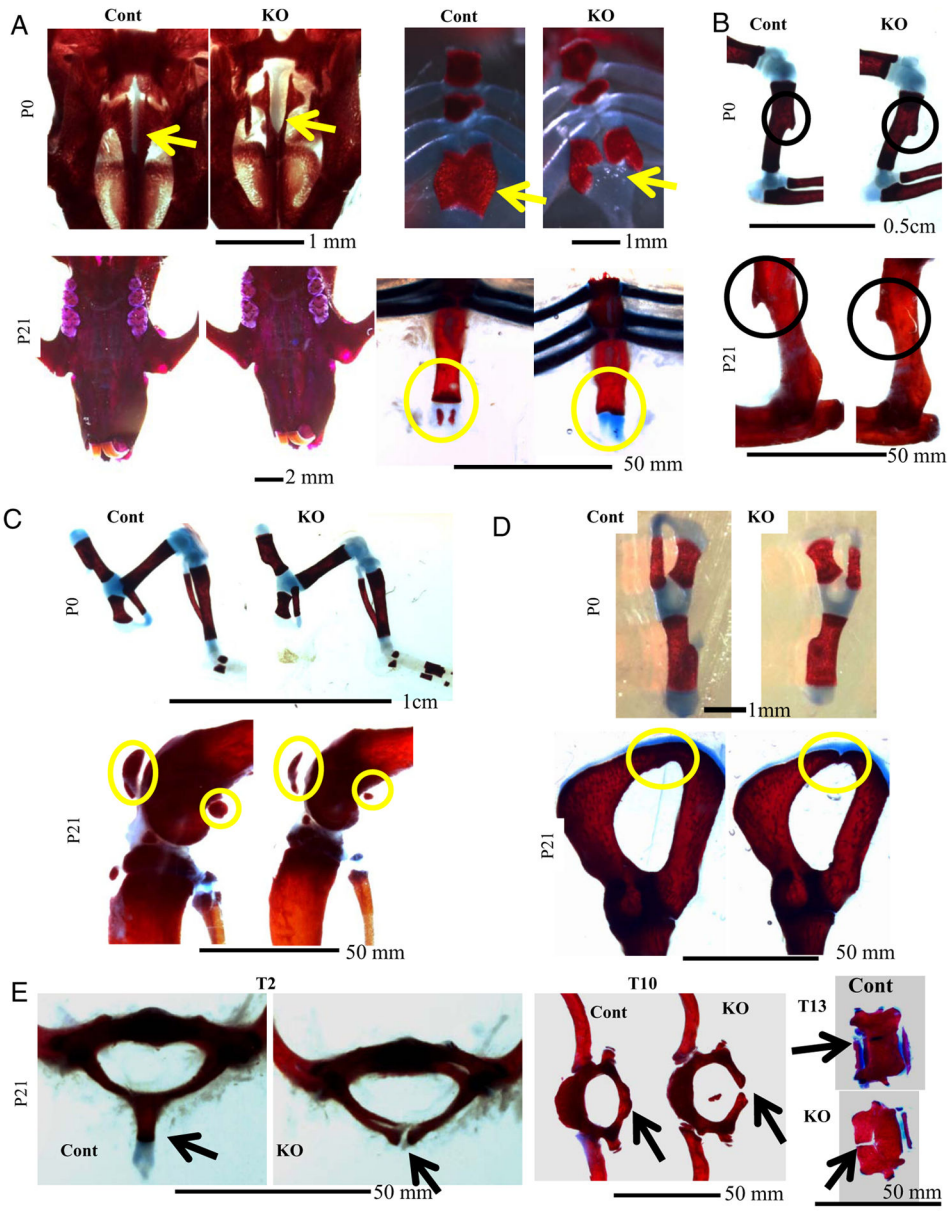

Figure 3.

Delayed Skeletal Development and Ossification in *Col1a1-Gsk3b* KO Mice Panels A–E show Alizarin Red (bone) and Alcian Blue (cartilage) staining of skeletal elements, comparing control (Cont) and skeleton-specific GSK-3β knockout mice (KO): A, (top left), P0 hard palate; A (top right), P0 sternum; A (bottom left), P21 hard palate; A (bottom right), P21 (Xyphoid process circled). B, Deltoid tuberosity; B (top), P0; B (bottom), P21. C, Knee joint. C (top), P0; C (bottom), P21. D, Pelvic bone. D (top), P0; D (bottom), P21. E, (left), T2 vertebrae; E (middle), T10 vertebrae; E (right), T13 vertebrae.

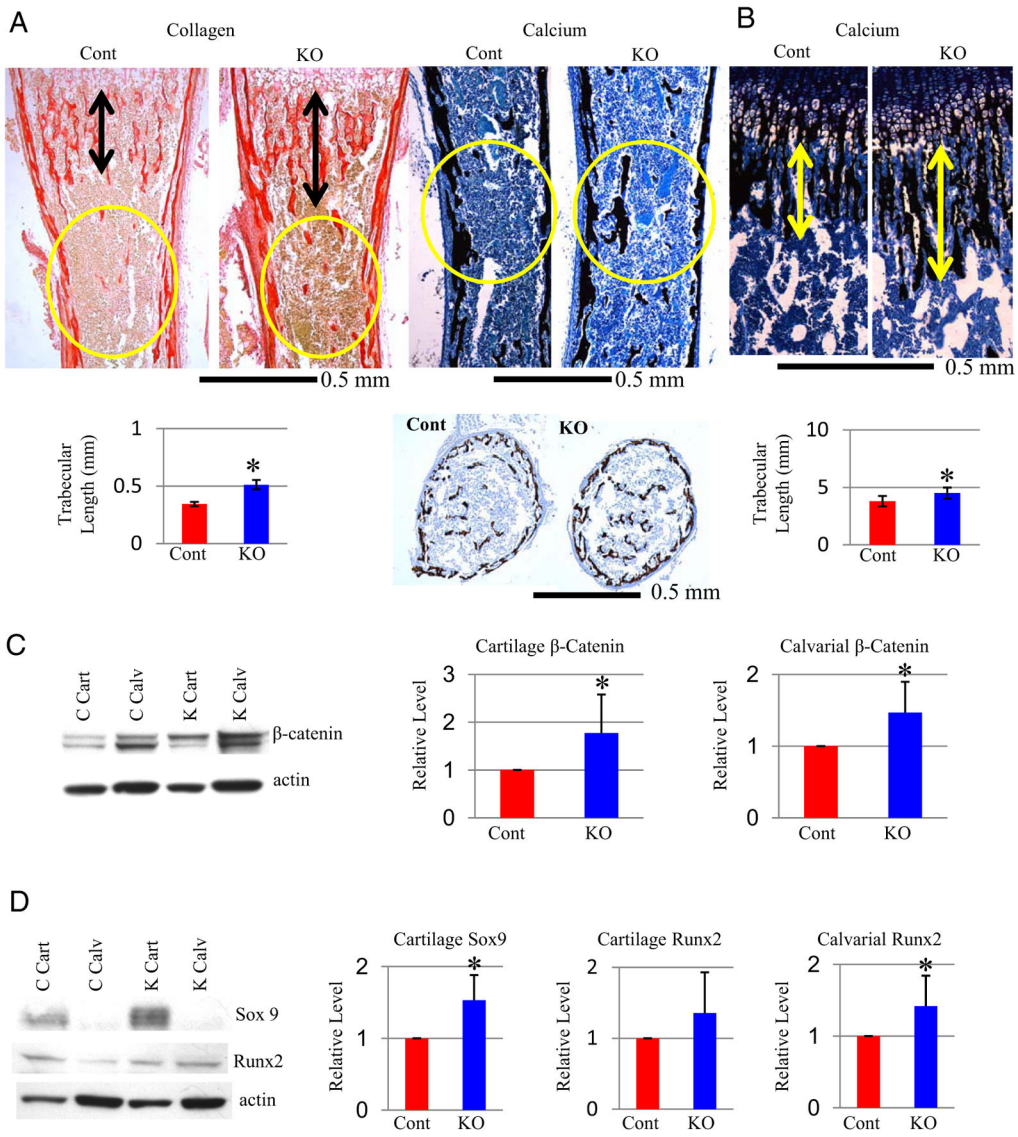

Figure 4.

Increased Bone Formation and Expression of Key Transcription Factors in *Col1a1-Gsk3b* KO Mice A, Analyses of bone formation in P0 tibias. A (top left), Picrosirius Red stain (fibrillar collagen). A (bottom left), length of trabeculae (black arrows) (n = 7). Increased middiaphysis trabecular bone (circled) was observed in KO mice. A (top right), VonKossa/ toluidine blue stain (calcification). Increased mid diaphysis (circled) was observed in KO mice. A (bottom right), Comparison of transverse sections stained with Von Kossa/toluidine blue in the tibia middiaphysis. B, P21 tibia sections stained with Von Kossa/toluidine blue showing longer trabeculas in KO mice, marked with arrows (top) and quantified (n = 4) (bottom). C, Analyses of β-catenin protein. C (left), Western blot analyses with β-catenin antibody (loading control β-actin) from cartilage (Cart) and calvarial (Calv) extracts of control (C) and knockout (K) mice. C (right), Quantitative densitometry; data normalized to control sample for cartilage (n = 8) and calvariae (n = 7). D, Analyses of Runx2 and Sox9 protein. D (left), Western blot analyses with Runx2 and Sox9 antibodies (loading control β-

actin [A]) from cartilage (Cart) and calvarial (Calv) extracts of control (Cont) and knockout (K) mice. D (right), Quantitative densitometry (n = 8). Quantitative data were compared using *t* test analysis; significant differences are denoted by asterisk (*, $P < .05$).

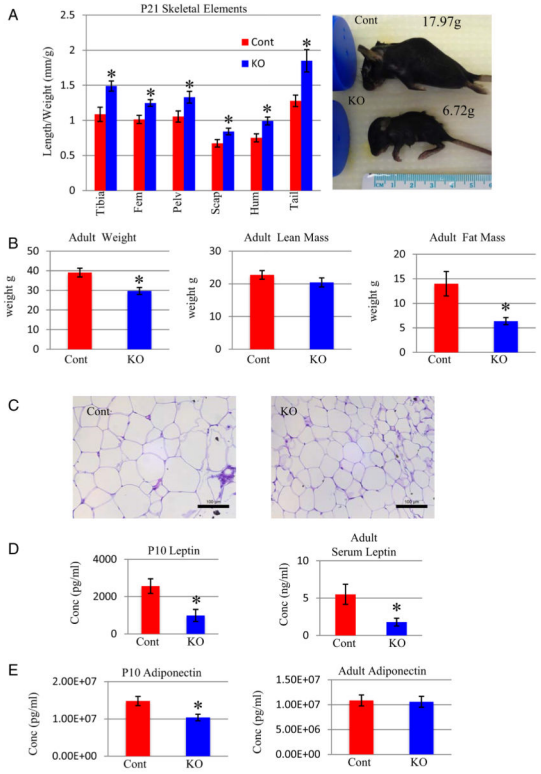

Figure 5.

Body Composition in *Col1a1-Gsk3b* KO Mice A (right), Length of skeletal elements proportional to animal weight for *Col1a1-Gsk3b* KO (KO) mice compared with control littermates (Cont) (n = 4). A (left), An example of a severely underweight mutant mouse (60%) with limb and skull sizes not proportional to its low weight. B, Quantification (QMR) of total mass (left), lean mass (middle), and fat mass (right) (n = 5) of adult mice, 2 littermate pairs of males and 3 littermate pair of females. C, Histology of epididymal adipocytes shows reduced cell size in KO mice. D, Analysis of serum leptin (Millipore Multiplex) in *Col1a1-Gsk3b* KO and control mice at P10 (n = 5) and adult mice (n = 8). E, Analysis of serum adiponectin (Millipore Multiplex) in *Col1a1-Gsk3b* KO and control mice at P10 (n = 5) and in adult mice (n = 10). Quantitative data were compared using *t* test analysis; significant differences are denoted by asterisk (*, $P < .05$).

A

Sex	Driver	Age	Test	Cont (mol/l)	SEM	KO (mol/l)	SEM	n	p	Sig
	Col I	P0	Fed	4.10	0.55	3.24	0.71	6	0.0041	**
	Col II	P0	Fed	3.93	0.13	3.73	0.15	11	0.3326	NS
Female	Col I	Adult	Fasted	5.53	0.23	4.38	0.27	10	0.0050	**
Female	Col I	Adult	Fed	6.22	0.14	5.76	0.15	16	0.0363	*
Male	Col I	Adult	Fasted	5.29	0.30	5.50	0.55	7	0.7377	NS
Male	Col I	Adult	Fed	7.34	0.35	6.04	0.36	11	0.0171	*

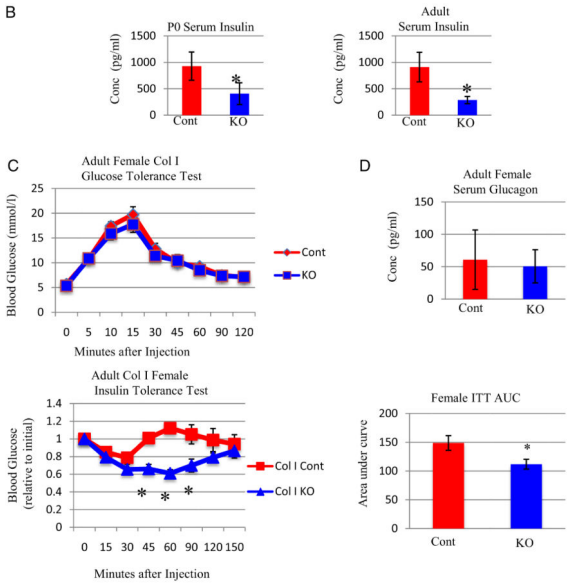

Figure 6.

Col1a1-Gsk3b KO Mice Have Decreased Blood Glucose, Serum Insulin, and Increased Insulin Sensitivity A, Blood glucose levels (mmol/L) of both Col1a1- and Col2a1-GSK-3β KO (KO) at P0 and adult mice (2–6 months) in both the fasted (6 hours) and random fed (Fed) states for both male and female mice. B, Analysis of serum insulin (Millipore Multiplex) in control (Cont) and knockout (KO) mice at left (P0 [n = 3]) and right (adult mice [n = 8]). C, (top), GTT results for *Col1a1-Gsk3b* KO (KO) and control littermates from adult female mice. C (bottom left), ITT results for *Col1a1-Gsk3b* KO (KO) and control littermates. C (bottom right), Area under the curve (AUC) analysis for the ITT of the *ColI-Gsk3b* KO and control mice. D, Analysis of serum glucagon (Millipore Multiplex) in control (Cont) and knockout (KO) adult female mice. Quantitative data were compared using two-way ANOVA or *t* test analysis, significant differences are denoted by asterisk (*, $P < .05$).

A

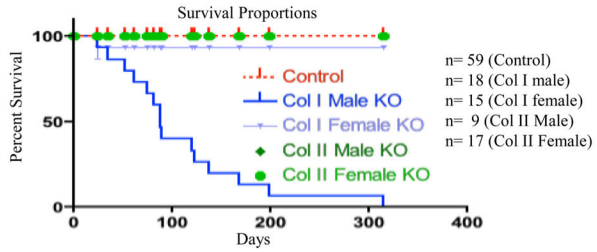

B

Sex	Driver	Age	Test	Cont (mol/l)	SEM	KO (mol/l)	SEM	n	p	Sig
Male	Col I	Prior to Death	Fed	6.33	0.85	12.18	1.86	4	0.0287	*

C

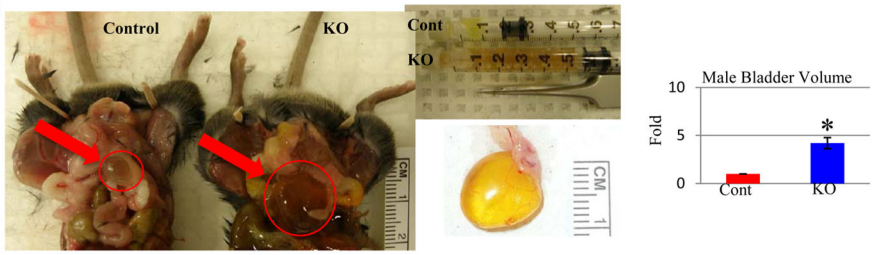

D

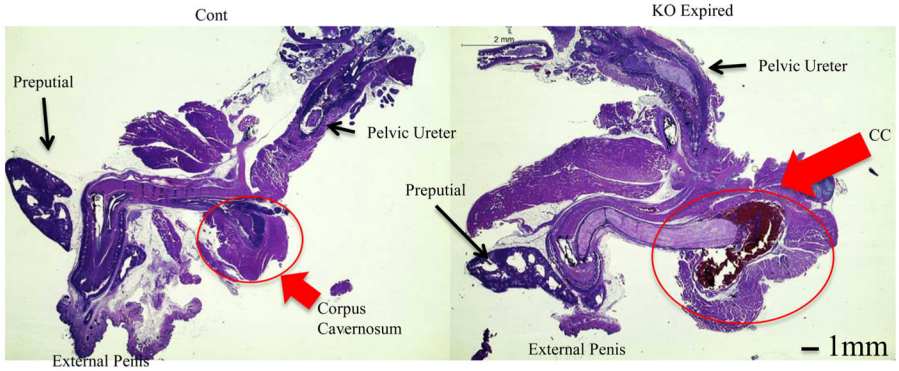

Figure 7.

Elevated Blood Glucose, Urogenital Tract Damage, and Premature Death in Male *Col1a1-Gsk3b* KO Mice A, Survival curves (Kaplan-Meier Plot) of both male and female of *Col1a1-* and *Col2a1-Gsk3b* KO mice tracked for 1 year. B, Data for male mice that had a glucose reading 1–2 weeks prior to premature death. C, Comparison of bladder size from male *Col1a1-Gsk3b* KO (KO) mice that died prematurely relative to age-matched control (Cont) littermates. B (top middle), Urine extracted from bladders of KO mice by syringe. B (right), Comparison of bladder volume (n = 4). B, Examination of male urogenital tract of a male *Col1a1-Gsk3b* KO (KO) mouse that died prematurely compared to control littermate (Cont). Hematoxylin and eosin staining of the urogenital tract showing a blood-filled corpus cavernosum (CC) in mutant mice (circled). Quantitative data were compared using *t* test analysis, and significant differences are denoted by asterisk (*, $P < .05$).

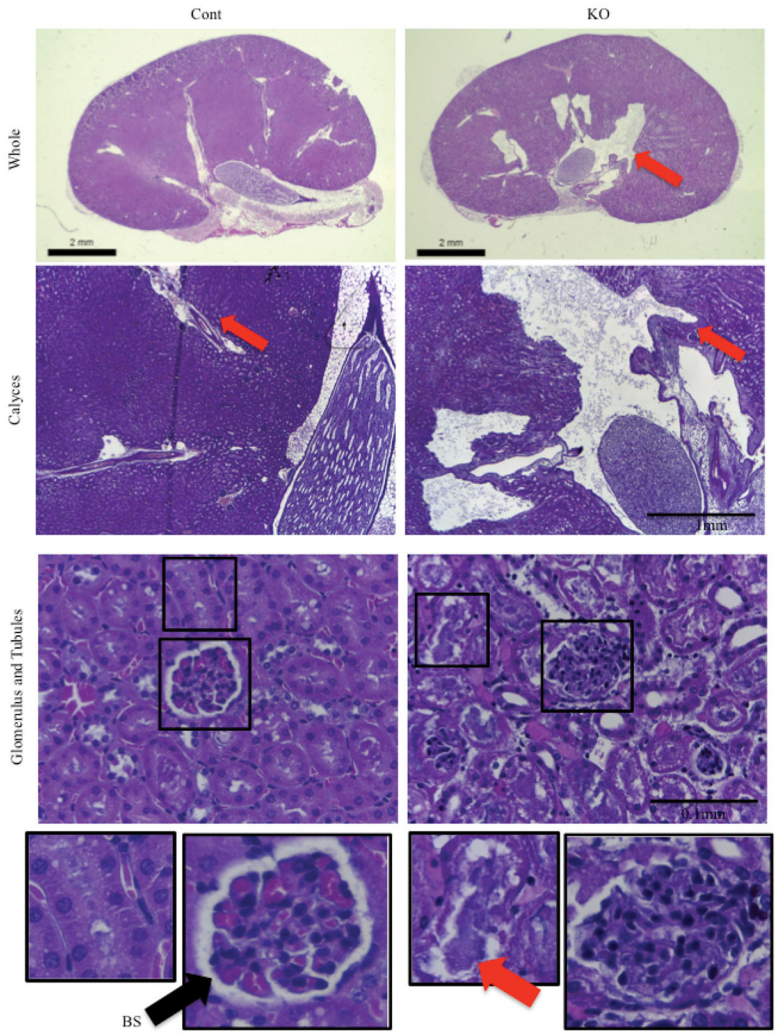

Figure 8.

Evidence of Kidney Damage and Hydronephosis in Male *Col1a1-Gsk3b* KO Mice Top, Hematoxylin and eosin staining of the kidney of a male *Col1a1-Gsk3b* KO (KO) that died with a severely distended bladder compared with control littermate (Cont). Figure shows various magnifications to display structures of the whole kidney and calyces. Arrows point to abnormally large spaces in the KO kidney. Bottom, H&E staining of the renal cortex from a male *Col1a1-Gsk3b* KO (KO) mouse that died compared with control littermate (Cont). Damaged renal tubules are full of proteinaceous material (red arrow). The Bowman's space (BS) is poorly defined in the KO glomerulus compared with the control (black arrow).